Bibliographic record: Nyman, L., Kestilä, A., Porri, P., Pudas, M., Salmi, M., Silander, R., Miikkulainen, V., Kaipio, M., Kallio, E. and Ritala, M., 2021. Constructing Spacecraft Components Using Additive Manufacturing and Atomic Layer Deposition: First Steps for Integrated Electric Circuitry. Journal of Aerospace Engineering, 34(5), p.04021049.
Bibliographic record link: https://doi.org/10.1061/(ASCE)AS.1943-5525.0001298

Constructing Spacecraft Components Using Additive Manufacturing and Atomic Layer Deposition – First Steps for Integrated Electric Circuitry

Leo Nyman[1], Antti Kestilä[2], Paavo Porri[3], Marko Pudas[4], Mika Salmi[5], Rudolf Silander[6], Ville Miikkulainen[7], Mikko Kaipio[8], Esa Kallio[9], and Mikko Ritala[10]

[1]Ph.D. Student, School of Electrical Engineering, Aalto University, P.O. Box 15500, FI-00076 Aalto, Finland (corresponding author). Email: leo.nyman@aalto.fi

[2]Dr.Tech., Researcher, Finnish Meteorological Institute, Dynamicum Erik Palménin aukio 1, FI-00560 Helsinki, Finland. Email: antti.kestila@fmi.fi

[3]M.Sc., Engineer, VTT Technical Research Centre of Finland, Tietotie 4E, FI-02150 Espoo, Finland. Email: paavo.porri@vtt.fi

[4]Dr.Tech., IP Manager, Picosun Oy (Ltd.), Tietotie 3, FI-02150 Espoo, Finland. Email: marko.pudas@picosun.com

[5]D.Sc., Staff Scientist, Department of Mechanical Engineering, Aalto University, P.O. Box 14100, FI-00076 Aalto, Finland. Email: mika.salmi@aalto.fi

[6]M.Sc., Research Assistant, School of Electrical Engineering, Aalto University, P.O. Box 15500, FI-00076 Aalto, Finland. Email: silander.r@gmail.com

[7]Ph.D., University Teacher, School of Chemical Engineering, Aalto University, P.O. Box 16100, FI-00076 Aalto, Finland. Email: ville.v.miikkulainen@aalto.fi

[8]Ph.D. Student, Department of Chemistry, University of Helsinki, P.O. Box 55, FI-00014 University of Helsinki, Finland. Email: mikko.kaipio@helsinki.fi

[9]Prof., School of Electrical Engineering, Aalto University, P.O. Box 15500, FI-00076 Aalto, Finland. Email: esa.kallio@aalto.fi

[10]Professor of Inorganic Materials Chemistry, Department of Chemistry, University of Helsinki, P.O. Box 55, FI-00014 University of Helsinki, Finland. Email: mikko.ritala@helsinki.fi

ABSTRACT

Many fields including the aerospace industry have shown increased interest in the use of plastics to lower the mass of systems. However, the use of plastics in space can be challenging for a number of reasons. Ultraviolet radiation, atomic oxygen and other phenomena specifically associated with space cause the degradation of polymers. Here we show a path towards creation of space-grade components by combining additive manufacturing (AM) and atomic layer deposition (ALD). Our method produced ALD Al_2O_3 coated thermoplastic parts, suitable for space applications. The highlight of this work is a significant reduction in outgassing, demonstrated using residual gas analyzer (RGA) sampling. Compared to uncoated parts, the ALD-Al_2O_3 coating decreased the outgassing of polyether ether ketone (PEEK), acrylonitrile butadiene styrene (ABS), polycarbonate (PC) and nanodiamond-doped polylactide (ND-PLA) by 46%, 49%, 58% and 65% respectively. The manufacturing method used in this work enables the use of topology optimization already in the early concept creation phase. The method is ideally suited for spacecraft applications, where the volume and mass of parts is critical, and could also be adapted for in-space manufacturing.

Keywords Spacecraft, atomic layer deposition, additive manufacturing, material extrusion, fused filament fabrication, fused deposition modeling

INTRODUCTION

The small-satellite market has rapidly expanded due to increasingly frequent launch opportunities and reduced payload costs. Currently, the capabilities of small satellites, such as CubeSats, are restricted in many ways, especially for active microwave instruments (Grau 2019). This is because the power requirements for such instruments easily exceed the amount of electrical power generated by the solar cell arrays of small satellites, even though the solar cells themselves are thin enough to be packaged in large numbers into a small volume. However, this is difficult in practice, since foldable structures require space and complicate the routing of electric connections. Also, additional engineering is required, in order to make the structure of foldable solar cell arrays able to withstand mechanical loads. One approach for overcoming these challenges is to combine

additive manufacturing (AM) and atomic layer deposition (ALD), to construct large foldable solar cell array assemblies based on integrated electric circuitry. If these were manufactured in orbit, the system mass and volume could be further reduced, since the microgravity environment would be more benign to the structures. In addition, this combined AM-ALD production process would allow efficient use of promising new concept creation techniques, such as topology optimization, which would enable further reductions in the mass of such structures. Many fields including the aerospace industry have shown increased interest in the use of plastics to lower the mass of systems (Kutz 2002, p. 336). However, the use of plastics in space can be challenging. Hence overcoming these challenges is of critical importance.

The space environment is destructive for many thermoplastics. Materials with high outgassing in a vacuum are typically excluded from spacecraft designs. When moving outside of the Earth's protective atmosphere and magnetosphere, many materials are degraded by high-flux ionizing radiation across a wide spectrum. Ultraviolet radiation (UV) affects the top surface layers and has sufficient energy to break the C–C, C–O and other polymer bonds (Grossman and Gouzman 2003). Other radiation species penetrate materials to such a high degree that surface coatings alone cannot provide comprehensive protection. In space, the temperature range can be extreme, depending on the location of the component in a spacecraft (Gilmore 2003). This makes some materials brittle or elastic, resulting in mechanical failure. Each material has a unique coefficient of thermal expansion (CTE). When materials with different CTE are joined together to form a structure, thermal stresses and cycles cause non-equal expansion or contraction of parts, causing failures if not taken into account in the design. Apart from CTE, the concentration of atomic oxygen (AO) limits the choice of materials particularly for low Earth orbit (LEO) satellites, due to its highly reactive nature (Cruise et al. 2006) and relatively high concentrations, which can reach up to $9 \cdot 10^{21}$ atoms/cm^2 in LEO (Stein 1993). Indeed, a long duration exposure facility (LDEF) experiment on an LEO satellite demonstrated that no polymeric material can be completely resistant to atomic oxygen and UV-inflicted erosion (Stein 1993). LDEF findings have shown that the combination of AO and UV eroded uncoated graphite-epoxy surfaces on the leading edge structure (Stein 1992). Atomic layer

deposition (ALD) has been proposed for protecting polymers in space (Minton et al. 2010) and recently the combination of AM and ALD has been studied (Kestilä et al. 2018). These studies were partly driven by the capability of ALD to create conformal coatings over parts with complex shapes or sharp edges. When properly designed and applied, the conformal ALD coating provides an excellent gas barrier and UV shield.

Coatings for Spacecraft

Many metals and oxides protect against AO. However, since silver and copper can be degraded by AO, these should not be implemented in the outer layer. The LDEF experiment (Stein 1993) showed that cracks and holes in the coating allow AO to attack the underlying polymer. The associated undercutting process erodes the polymer material under the coating near the coating defect (Stein 1992). Even a thin coating (e.g., 120 nm) of some inorganic material, such as aluminum, nickel or silica, can provide excellent protection with good adhesion. An important property of these thin-film overcoatings is their resistance to crazing (Stein 1992). A related finding from LDEF was that surface micro-cracking was influenced by the thermal cycling temperature range.

When the International Space Station (ISS) was designed, the LDEF results were useful in the design work. The Kapton solar array blankets manufactured for the ISS were coated on both sides with 130 nm of SiO_2 for protection against AO. Recently, ALD coatings have been used to protect polymers for usage in spacecraft (Minton et al. 2010). This study used Al_2O_3 to provide protection against AO, and another layer of TiO_2 to block damaging UV radiation. Another good UV-shield material is ZnO. A coating thickness of approximately 35 nm of Al_2O_3 provided protection against AO. However, some substrate materials, such as FEP (fluorinated ethylene propylene or Teflon®), required a thicker coating for efficient protection, most likely caused by the different film-forming mechanisms of ALD Al_2O_3 on various substrate materials (Tynell and Karppinen 2014; Cooper et al. 2008).

Spacecraft components may be exposed to large temperature ranges. It is commonly known that coatings are susceptible to cracking, if the CTE values differ greatly between the coating material and underlying substrate. Therefore, materials with similar CTE values are preferred.

Coating thickness also plays a role. The negative effects of cracking will depend on the application. For example, when an Al_2O_3 ALD film is used as a gas diffusion barrier, cracks will degrade its efficiency (Jen et al. 2011). Several studies have shown that for hard coatings, thinner films are less susceptible to cracking (McGuigan et al. 2003).

Atomic Layer Deposition

ALD is a type of chemical vapour deposition (CVD) technique. This paper focuses on an Al_2O_3 coating, a well-known ALD process. Other relevant materials are briefly discussed when appropriate. Al_2O_3 is well suited for coating of polymers, partly because it can be deposited over a wide process temperature range. In earlier studies, Al_2O_3 has been deposited at temperatures ranging from 500 °C to as low as 33 °C (Groner et al. 2004). Due to their low glass transition temperatures (T_g), many polymers require relatively low process temperatures. On the other hand, the CTE of Al_2O_3 is very low compared to most polymers. This must be taken into account, since large difference in CTE between the substrate and the coating will induce cracking during thermal cycling.

As-deposited ALD Al_2O_3 is known to be amorphous and easily dissolvable into water. This type of amorphous coating structure has been shown to possess excellent gas barrier properties (Heidary and Randall 2015). However, the coating shall be protected from water and high levels of humidity. Degradation of ALD Al_2O_3 has been reported after exposure to liquid water or high-temperature and high-humidity environment (124 °C, 95 % rH) (Abdulagatov et al. 2011; Rückerl et al. 2017). In general, non-corrosive environment is provided for spacecraft components before and during launch. Broas (2018) reports, that an ALD deposited Al_2O_3 coating may be subjected to tensile stresses. This is at least partly caused by the CTE difference of the substrate and the coating. Tensile stress can lead to cracking and delamination of the coating.

The outcome of the film deposition is subject to many quality factors. Properties such as amount and type of impurities, film phase (crystallinity), stoichiometry, stress state, film uniformity, thickness, interface structure and conformity are more or less important, depending on the application (Broas 2018). Regarding distinct polymer layers (structural or functional, e.g. electrically conduct-

ing), interfacial adhesion between layers must be ensured (Varadan et al. 2001, p. 16). Naturally, this adhesion requirement also applies for ALD layers.

For spacecraft, the evaporation of any condensable volatiles may adversely contaminate optical sensors (Fortescue et al. 2011, p. 40). One benefit of using ALD in the encapsulation of polymers is that prior to the coating process the substrates are evacuated and heated to the deposition temperature. This *stabilization time* effects a degassing of the part. Further, the ALD coating is then deposited while the substrates are hot, dry and in a vacuum, as they are in space. As a result, the ALD coating reduces outgassing of the polymer part in space. The ALD barrier coating can also prevent gas absorption from ambient atmosphere, before the satellite is delivered to orbit where it will operate.

Another possible use case for ALD is the inhibition of tin whiskers. This is a known phenomenon, causing complications in the design and manufacturing of space-grade electronics. Until now, the solution has been the use of lead-tin alloys for soldering, where Pb provides mitigation against the growth of tin whiskers. However in the European Union, legislation to ban lead-tin alloys is moving ahead. Therefore the use of Al_2O_3 ALD coating is one promising lead-free alternative to inhibit tin whisker growth in space-grade electronics (Kutilainen et al. 2019).

METHODOLOGY

This section explains how the test articles were made and the test setup used. All results and conclusions are shown in later sections.

For the experiments, thin–film coated thermoplastic parts were manufactured using AM, epoxy impregnation and ALD. The fabricated parts were tested to determine outgassing properties. For AM, material extrusion (MEX) was used.

The first phase of the research focused on finding suitable thermoplastics, taking into account the space environment and potential use cases. Based on our tests and a literature review, a list of promising material candidates for space applications was created. The list included polyether ether ketone (PEEK), polycarbonate (PC), nanodiamond doped polylactide (ND-PLA) and polyimide (PI, Kapton®). As the melting of polyimide is highly problematic, it was not considered for this

study as it was not possible to use it with our AM process. Instead acrylonitrile butadiene styrene (ABS) was included in our list of potentially viable test materials. Finally, the following four thermoplastics were selected as substrate materials for this study.

ABS was used in the ISS *Made in Space* experiment (Prater et al. 2019). It is a widely used material with many good properties (Kutz 2002, p. 339). ABS has good mechanical properties, but the usable temperature range is low. At low temperatures ABS may become brittle, however it does posses a good radiation tolerance (Shulman and Ginell 1970).

PC is used in many industries, including aerospace. The following has been reported (Mark 2009, p. 480): *"The polymer has an excellent balance of high heat resistance, stiffness, strength, dimensional stability, low creep, ignition resistance, and exceptional impact strength"*. The radiation tolerance and outgassing properties of PC are sufficient for space applications. PC has been widely used in space suit helmet visors. It has also been used in space-based science instruments (Kirn 2013).

PEEK is an aerospace-grade high-strength material. It has good mechanical properties over a wide temperature range. PEEK has a good tolerance to radiation and it is suitable for relatively high temperature environments, compared to other plastics. It also has good (low) outgassing properties for space applications and water absorption is low (Murari et al. 2002). PEEK has been used in the main structure of the ISS remote manipulator arm, as a matrix for the carbon fibre composite (Lanouette et al. 2015). It has also been proposed as a candidate material for the manufacturing of spare parts and other items in orbit, using AM (Zanjanijam et al. 2020). Initially, these items will mostly be used inside pressurised habitats. Due to the excellent mechanical properties of PEEK, it can also find good use cases outside habitats. If this will be the case, robust protective coatings will be beneficial in protecting such exposed parts from the degrading effects of the space environment.

ND-PLA Carbodeon uDiamond PLA® is a special nanodiamond doped polylactide filament for material extrusion. In particular, the addition of nanodiamonds can improve the mechanical properties of PLA filaments used in *3D printing*. It also results in improved thermal conductance of the plastic material (VTT 2018). Plain PLA has a fair level of radiation tolerance (Krzysztof et al. 2011). In 2019, Tethers Unlimited and NASA installed the *Refabricator* device on ISS. This device is capable of recycling PLA waste material and 3D printing new parts from it (Prater et al. 2019). PLA can be readily utilised for printing generic items used inside space habitats. At this moment, it is difficult to predict how extensively PLA parts will be used in the vacuum of space. A robust protective coating will be a key enabler for such use cases. In light of recent studies, the use of printed PLA parts in vacuum looks promising (Johnson et al. 2020; Nogales et al. 2018).

Figure 1. CAD model for the test articles. The outer dimensions of this part were 46 × 23 × 2.6 mm. The coordinate axes shown were used in the material extrusion machines.

Step 1 – Design and Additive Manufacturing of Test Articles

The geometry of the test articles was designed with Autodesk Fusion 360 CAD software and exported as an *.stl* file (Fig. 1). This was further refined (sliced) into G-code files using Intamsys IntamSuite 3.2.0 and Ultimaker Cura 3.5.0 software. The outer dimensions of this part were 46 × 23 × 2.6 mm. The part geometry and features were designed in a way to mimic a typical small circuit board, having a placeholder for a microcontroller (Texas Instruments® MSP430) and areas for electrically conductive tracks in three dimensions (3D). The 3D features included holes and

small tunnels. One end of the part was designed as a custom 5-pin connector, enabling a quick connect and disconnect to external electric circuits. The part design was created for the purpose of testing 3D electric circuit manufacturing using AM and ALD. It was envisioned that a follow-up research would add area-selective ALD-copper layers to create the conductive tracks.

The ABS and PEEK parts were printed with an Intamsys Funmat HT, while PC and ND-PLA parts were printed with an Ultimaker 3 (Fig. 2). For the ABS, PC and ND-PLA parts, a *Dimafix*® glue pen was applied on the build platform to improve adhesion. The much higher bed temperature of the PEEK printing, however, required a different adhesive. After trials, a *Tresemme*® hairspray was used to improve the build-plate adhesion. Table 1 and Table 2 contain a summary of the print parameters used. The parts were printed flat on the build platform, so that the top surface normal was pointing along the printer Z-axis. No raft or brim was used, except for the PEEK parts, which had a 14 mm wide brim. The brim was removed by cutting, after the part had been removed from the printer.

Step 2 – Epoxy Impregnation

Epoxy impregnation was used to reduce the inherent porosity of the AM parts. Panacol® Vitralit 2008 and Vitralit 2009F epoxies were selected for this purpose. Both are ultraviolet (UV) and thermally curable compounds. For simplicity, an impregnation without a vacuum chamber was chosen. At first, the test articles were cleaned using isopropanol wipes. The impregnation was performed by first pouring Vitralit 2008 and Vitralit 2009F into separate Petri dishes. The test articles were then placed and submerged into the selected epoxy, as per Table 3. This table also shows those test articles for which the epoxy impregnation was omitted. During impregnation, the epoxies, dishes and test articles were at room temperature inside a ventilated lab cabinet. Mechanical vibration was applied to the dishes, in order to enhance the removal of air bubbles. The parts were then lifted and excess uncured epoxy was allowed to drip off. Pressurised air was used to remove uncured epoxy from small holes and cavities. The parts were then cured using an Osram® Ultra-Vitalux 300 W UV lamp, which provides approximately 13.6 W of power in the wavelength range between 315 nm and 400 nm. The distance to the lamp was approximately 20 cm and each surface was illuminated for two hours. The second curing step was performed in an oven, where

227 the parts were heated at 105 ˚C for 30 minutes. The oven was not fitted with a UV light source.

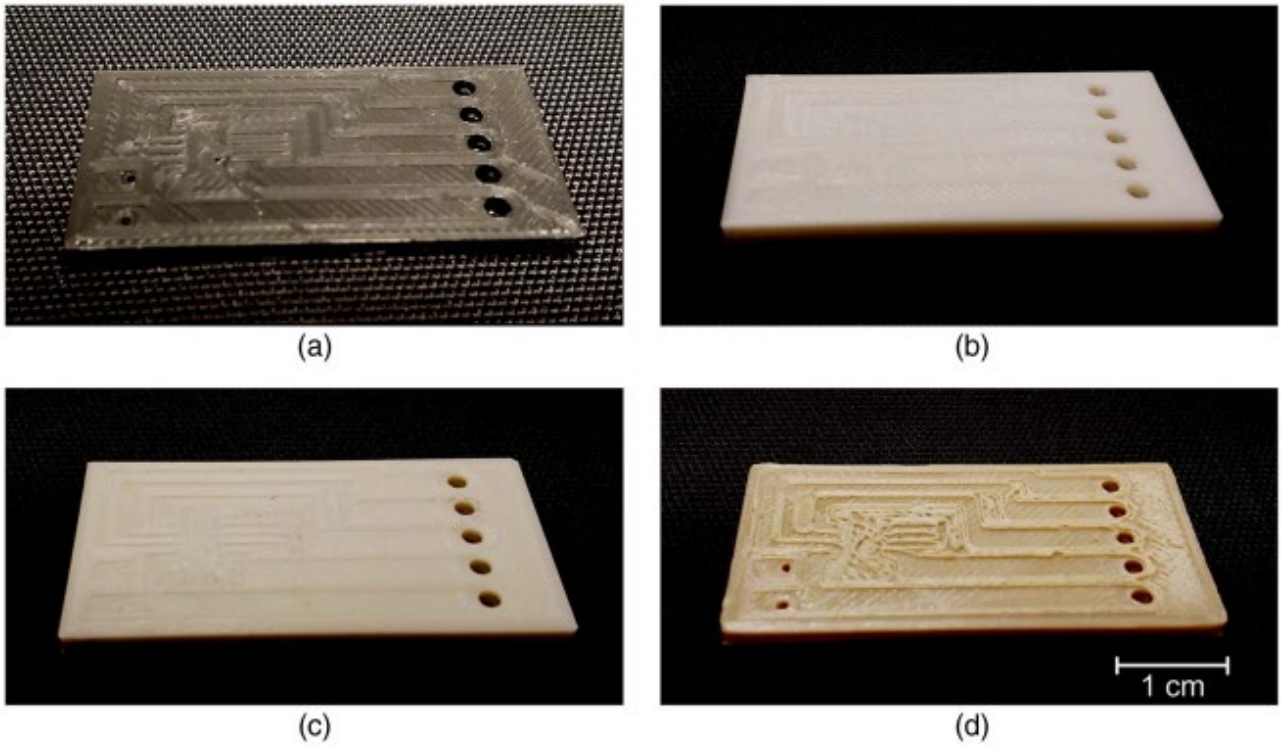

Figure 2. Test articles manufactured with material extrusion printers: (a) ABS part; (b) PC part; (c) ND-PLA; and (d) PEEK. According to visual inspection, the ABS and ND-PLA printing gave the best results in terms of fine details (actual print resolution). The noticeable warping of the part and somewhat crude details.

Table 1. Temperatures, print speed, and bed glue used in the MEX process

Device	Material	T_{BED} (°C)	$T_{CHAMBER}$	T_{NOZZLE} (°C)	Print speed (mm/s)	Bed glue	Part dimensions (mm)
Funmat HT	ABS	95	90°C	240	50	Dimafix	45.95 × 23.20 × 2.50
Funmat HT	PEEK	160	90°C	400	6	Tresemme	46.10 × 23.15 × 2.55
Ultimaker 3	PC	100	unheated	270	50	Dimafix	45.85 × 23.15 × 2.65
Ultimaker 3	ND-PLA	60	unheated	230	50	Dimafix	46.20 × 23.60 × 2.55

Note: T_{BED} = temperature of the build plate; $T_{CHAMBER}$ = temperature of the print chamber of the printer used; and T_{NOZZLE} = temperature of the printer's extrusion nozzle. A much slower print speed was used for the PEEK parts. The last column shows actual part dimensions, as measured using a vernier caliper.

Table 2. Diameters and other settings for material extrusion

Device	Material	D_{NOZZLE} (mm)	Gap (bed-nozzle)	RAFT/BRIM	Material flow (%)	Print fan
Funmat HT	ABS	0.4	Leveling card	None	100	On
Funmat HT	PEEK	0.4	0.35 mm	Brim, 14 mm wide	105 for initial layers, then 100	Off
Ultimaker 3	PC	0.4	Leveling card	None	100	Off
Ultimaker 3	ND-PLA	0.4	Leveling card	None	100	Off

228 **Step 3 – ALD Al_2O_3 Coating**

229 Selected test articles (Table 3) were coated with ALD-alumina as follows. The parts were
230 cleaned with isopropanol alcohol wipes and dried with clean compressed air, then placed inside a

R150 ALD reactor (Picosun Oy, Finland) for the first coating layer. The coating process started with an initial phase of 24 hours of thermo–vacuum baking at 90 ˚C, to remove moisture and other volatiles as much as practically possible. The same chamber temperature was maintained for the subsequent ALD coating process, with a vacuum of approximately 0.3 mbar. Because the test articles were thermoplastic parts, the ALD process temperature had to be limited, in order to avoid damaging the parts. Based on an earlier study (Groner et al. 2004), 90 ˚C was chosen as this gives near the maximum growth rate and is not too hot to severely damage the test articles.

A targeted thickness of 95 nm was selected for the ALD-alumina layer. In lack of better information of the thickness needed, thickness significantly exceeding the minimum used for barrier applications (Jen et al. 2011) was selected, but below the level which was known by experience to cause delamination issues due stress from CTE mismatch. To achieve this target thickness, the ALD cycle count was set to 1000.

Table 3. Substrate material, type of epoxy used for impregnation, estimated thickness of the ALD coating, and outgassing results for test articles

Test article label	Substrate material	Epoxy impregnation	ALD Al_2O_3 thickness (nm)	Outgassing results
A1	PEEK	Vitralit 2008	95	Not tested
A2	PC	Vitralit 2009F	95	Not tested
A3	ABS	Vitralit 2008	95	Not tested
A4	PEEK	Vitralit 2009F	95	Not tested
A5	ND-PLA	Vitralit 2008	95	Not tested
A6	ND-PLA	Vitralit 2009F	95	Not tested
A7	PC	None	95	Not tested
A8	PC	Vitralit 2008	95	Not tested
A9	PC	None	95	Not tested
A10	ABS	Vitralit 2009F	95	Not tested
A11	PC	None	95	Tested
A12	PEEK	None	None	Tested
A13	ND-PLA	None	None	Tested
A14	PC	None	None	Tested
A15	ABS	None	None	Tested
B1	ABS	Vitralit 2008/2009F	95	Not tested
B2	ND-PLA	Vitralit 2008/2009F	95	Tested
B3	ABS	Vitralit 2008/2009F	95	Tested
B4	ABS	Vitralit 2008/2009F	95	Not tested
B5	PC	Vitralit 2008/2009F	95	Not tested
B6	PEEK	Vitralit 2008/2009F	95	Tested

Note: The selection of epoxy was not recorded for Test articles B1–B6. These parts received either Vitralit 2008 or 2009F.

The ALD Al_2O_3 deposition was carried out using trimethylaluminium (TMA) and deionized water. The precursor dose times were 0.3 s for TMA and 0.2 s for water. Purge time was 60 s for both dose types to ensure egress of the reactants from the reaction chamber between pulses. This chemistry was selected, because it is known to produce films of high quality and good adhesion. Water is a common reactant for ALD-grown metal oxides, as it is gentle to the substrate surface (Johnson et al. 2014). Using this setup, a layer of ALD Al_2O_3 was then deposited on the epoxy

impregnated thermoplastic substrate or non-impregnated thermoplastic substrate as per Table 3.

Following the ALD coating, the parts were examined with an Olympus® BH-2 optical stereomicroscope. Images were captured using an Olympus® SC30 camera module attached to the microscope.

Step 4 – Thermal-Vacuum Outgassing Test

For the thermal–vacuum outgassing test, the ALD-coated parts A11, B2, B3 and B6 were selected. It should be noted that A11 was not epoxy impregnated, whereas the other three parts were epoxy impregnated (Table 3). This was so, because an associated coating test (not reported in this paper) consumed all the epoxy impregnated PC parts. Although not planned, this did provide an opportunity to see on a coarse level how a missing impregnation could affect the outgassing. The A11 part had only ALD Al_2O_3 coating on top of the polymer substrate.

Reference parts (A12, A13, A14 and A15) were selected and these were not epoxy impregnated nor ALD coated. These uncoated parts were manufactured using AM in the same way as for the coated parts and using the same G-code file.

All in all, eight test articles were tested for outgassing: four with an ALD coating and four reference parts with no ALD coating. The other parts listed in Table 3 were not included in the outgassing test. They were retained in the table, as they were relevant for other observations included in this paper, including the AM, ALD and impregnation.

Next, an outgassing test using an MKS Vision 2000-C quadrupole residual gas analyzer (RGA) and a thermal–vacuum chamber was conducted. For each of the four plastics (PEEK, ND-PLA, PC and ABS), the outgassing was measured for the uncoated part and coated part using the same setup.

The tests were conducted with a custom-made setup. The vacuum chamber was constructed from a KF-40 type T-shaped steel tubing component (Fig. 3). One open end of this T-tube was connected to the RGA. The second open end was fitted with an extension tube, which incorporated connections to a secondary vacuum pump, a manometer (MKS 722B Baratron), and a positive pressure dry nitrogen purge line. The third open end, of this T-shaped chamber, was fitted with a KF-40 stainless steel end cap with a clamp.

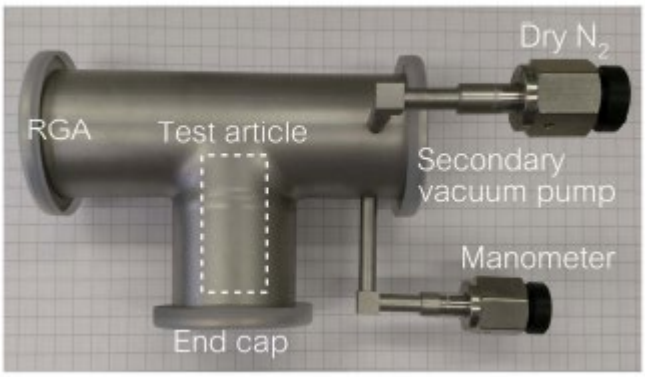

Figure 3. KF-40 steel thermal-vacuum chamber used in the outgassing tests. The secondary vacuum connection and nitrogen line were closed during the RGA measurements. The end cap opening was fitted with an Aldrich two-hand AtmosBag and a steel cap with a clamp. The test articles were first placed inside the nitrogen filled AtmosBag, and then placed from there inside the vacuum chamber via the end cap. The openable end cap also resided inside the AtmosBag. Using this setup, the test articles could be moved inside the vacuum chamber after base-line measurements, without contaminating the chamber with ambient air. The vacuum chamber tube diameter was 39.5 mm and flange outer dimension was 55.0 mm.

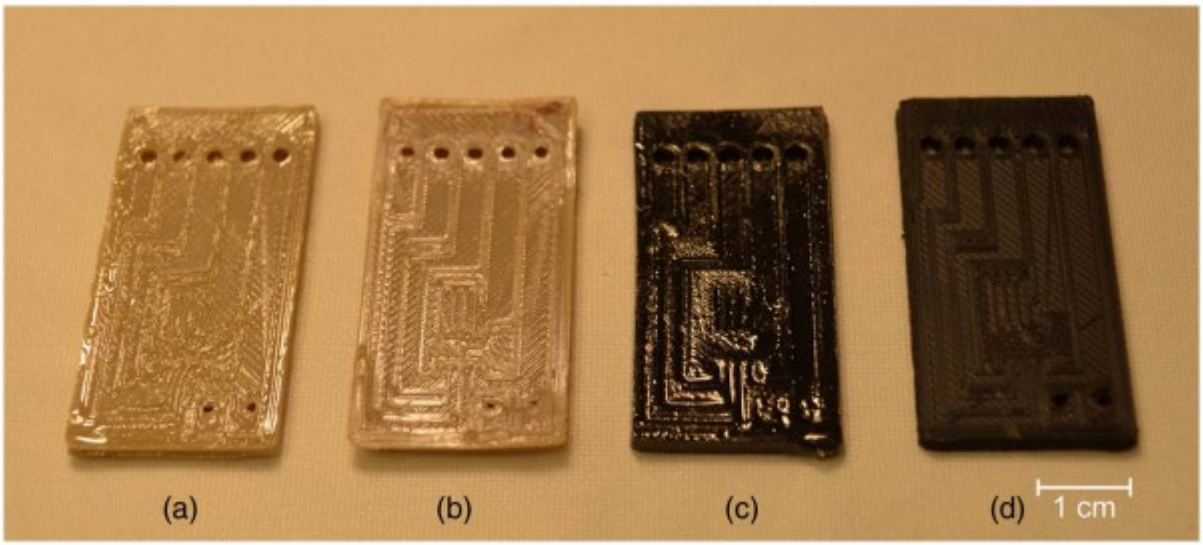

Figure 4. PEEK and ABS parts used in the outgassing test taken after the test runs: (a) coated PEEK; (b) uncoated PEEK; (c) coated ABS; and (d) uncoated ABS. The coating system comprised of epoxy impregnation (thickness > 1 μm), followed by ALD Al2O3 overcoat (thickness approximately 95 nm). The PC and ND-PLA parts were similar.

The vacuum chamber was then externally wrapped with

277 a heating wire element and a temperature sensor, both of which were connected to a digital heater
278 controller (Horst HT MC1). The outside of this assembly was wrapped using silicone insulating
279 mats and aluminum foil, in order to isolate the hot vacuum chamber from its surroundings as much
280 as possible. The role of the secondary vacuum pump was to provide a vacuum for purging, and
281 to get the chamber pressure below the threshold of the RGA's turbomolecular pump. During RGA
282 measurements, the secondary vacuum pump vent and nitrogen line vent were closed. This way, all

outgassing particles were routed via the RGA and into an external trap, forced by the turbomolecular pump of the MKS Vision 2000. During RGA measurements, the vacuum level was in the range of 0.02..0.89 mbar, depending on the amount of outgassing from the test article. The test flow was as follows:

1. The steel vacuum chamber was heated to 55 ˚C.
2. A baseline measurement was conducted with the chamber being empty.
3. The empty vacuum chamber was purged with dry nitrogen gas three times.
4. A coated test article was placed into the chamber (see Fig. 3 and Fig. 4), via an N_2 filled glove bag.
5. The vacuum chamber was purged with dry nitrogen gas three times, with the test article residing in the chamber.
6. A *coarse* resolution measurement was conducted using the RGA. This was labelled as TVC Test 1. The duration of this step was approximately 15 minutes. Only the recorded RGA data from the first 12 minutes and 55 seconds was used for the actual analysis. Using this cropping of data, exactly the same number of measurement cycles was analyzed for all the test articles.
7. Following the previous step, with the test setup running continuously, a *fine* resolution measurement was conducted using the RGA. This was labelled as TVC Test 2. The duration of this step was approximately 50 minutes, while the recorded RGA data from the first 45 minutes and 44 seconds, counted from the moment when RGA switched to fine resolution, was cropped for the actual analysis.
8. The test article was removed from the chamber.
9. An uncoated reference test article, made from the same thermoplastic as the coated test article in step 4, was placed in the chamber.
10. The vacuum chamber was purged with dry nitrogen gas three times, with the reference test article residing in the chamber.
11. RGA measurements were made in the same way as in steps 6 and 7.
12. The test article was removed from the chamber. End of the test. The steel vacuum chamber

was kept at 55 ˚C during all the steps shown above.

An identical test flow (as explained above) was used for each of the thermoplastics tested. The only exception was for the testing of the two ABS parts, where the uncoated part was moved into the chamber in step 4 and the coated part in step 9. This was done in order to evaluate whether the small deviation in the vacuum chamber temperature towards the end of a test run could affect the outgassing rate.

The collected RGA data was then analyzed as follows. The flux measurements of detected ion species were organized into a table, with scans (temporal range) representing Y-axis rows and particle mass range (1–300) forming X-axis columns. The average flux of each column was calculated. Static noise in the measurement data was detected by observing very small negative flux values. Based on this observation, a threshold value was set and columns having an average value below it were discarded as noise. These filtered average fluxes were then used to produce bar graphs and logarithmic mass spectrum plots as follows: For the bar graphs (Fig. 6 and 7), the constituents of N, N_2, H_2O, OH and O_2 were removed from the RGA data before analysis, as these were most likely traces of trapped ambient air and residuals of nitrogen gas used during chamber purging. For spacecraft design purposes, it is important to narrow down the data to the outgassing of condensable contaminants, in relation to the space environment. After this filtering, the average fluxes of the remaining columns were integrated and this value was used as the outgassing of the corresponding test article. For the logarithmic mass spectrum plots (Fig. 8), the same filtered data set was used. However, the constituents of N, N_2, H_2O, OH and O_2 were retained in this case, so that these peaks are visible in the mass spectrum plots. The logarithmic plots were only used for an RGA peak detection (qualitative analysis).

The *MKS Process Eye Professional* software outputs the data as *pressure in millibars*. However, a careful calibration process is needed if accurate values for partial pressures of ion species need to be obtained. Therefore, we report our measurements using an arbitrary unit (arb. unit). The reported values are not factored. We have simply replaced "millibar" with "arb. unit" in this paper.

RESULTS AND DISCUSSION

Here we report the results of the tests in the same order as they were introduced in the previous

section.

Results of Step 1 – Additive Manufacturing

In order to achieve proper adhesion between the printed part and the heated build platform, it is important to apply glue or another suitable compound on the platform before printing. Commercial 3D-printing build-surface sheets are also available. Kapton and other tapes are also used for this purpose. As the build plate temperature is increased, the choice of options gets narrower. These additives aim to ensure sufficient adhesion, ensuring a successful print. Also, they make the part removal easier after the print. This could otherwise be a challenge, especially for PC.

The manufacturing time of the ABS, PC and ND-PLA test articles was about 1 hour per part, regardless of the device used. The PEEK articles took about 2 hours to print. The pre-heating phase is longer and the print speed lower when using PEEK. Bed leveling and calibration is important, in order to ensure good quality and adhesion for the initial printed layers. We noticed that when using the Funmat HT with PEEK, the printer bed, chamber and nozzle must be pre-heated to operating temperatures before the bed leveling and calibration. Otherwise, the gap between the nozzle and the bed will not be correctly adjusted.

The measured dimensions of the AM parts, as they were removed from the printer and cleaned, are included in Table 1.

Additive Manufacturing with PEEK

PEEK was the most difficult of these materials to print successfully using material extrusion. The parts were initially always warping and detaching from the bed during printing. This was caused by thermal expansion and subsequent contraction. Different settings for the bed and nozzle temperatures were tried, without noticeable improvement. Dimafix®, UHU® polyvinylpyrrolidone (PVP) and Dremel® glue gun adhesives were trialled without success. Finally, a *Tresemme*® hairspray combined with a brim provided sufficient adhesion for the print. The hairspray was able to provide adhesion only for approximately 10 minutes, while the brim was printing. After this, the hairspray dried and no longer provided sufficient adhesion. Based on our trials, a better solution for bed adhesion in high temperature polymer printing is needed.

Other relevant parameters are listed in Tables 1 and 2. This setup produced partially successful

prints. Finished parts were still slightly warped, and the quality of fine details was inferior to the ABS prints, in particular. We expect that higher bed and chamber temperatures could reduce the warping of the PEEK prints. This was, however, not tested because the Intamsys Funmat HT was already operating with its highest bed and chamber temperature settings.

Results of Step 2 – Epoxy Impregnation

In several industrial processes, the porosity of manufactured parts is removed or reduced with the use of impregnation compounds. Earlier studies by our consortium had found issues with the porosity of AM prints, resulting in ALD layers depositing inside the porous cavities of test articles. This phenomenon is unwanted in many cases. For example, when creating electrically conductive surface paths with ALD Cu, any conductive material deposited in the porous cavities inside the part are an issue. To avoid this, an epoxy impregnation step was added between the AM and ALD processes. The assumption was that epoxy-impregnated AM prints would not exhibit the porosity issue in the ALD coating step.

The actual impregnation step revealed that the viscosity of the two epoxies used was too high, for the intended purpose. The viscosity controls, to a great degree, the impregnation capability and the thickness and uniformity of the epoxy coating. Our method of using pressurised air to remove any excess Vitralit compound before curing is an option, but it did not result in a uniform coating thickness. Other mechanical methods may also be used to enforce a thin and uniform epoxy film before the curing step. At the end of the research, a simple self-made *centrifuge* was tested. When an uncured epoxy coated AM print was attached to the centrifuge and rotated at 1500 rpm, excess epoxy was effectively removed and a smooth epoxy layer remained, ready for UV curing.

In general, the UV curing of the parts was easy. However, if a UV lamp generates heat significantly, it needs to be placed at a safe distance away, so that the polymer parts are not overheated and deformed. This increases the UV curing time. The use of cooling fans may possibly be able to mitigate this issue. When the parts were removed from the oven following the second curing step, we noticed that the ABS parts were slightly warped. This is not surprising, since the oven temperature exceeded the continuous use temperature of ABS, which is 80 ˚C. Overall, the impregnation was successful. We were able to successfully eliminate the porosity of

the AM prints, at least near the surface of the parts. This was evident based on visual inspection of the parts after impregnation (continuous layer of epoxy on the surface). Also, an inspection with an optical microscope after the ALD coating showed a bulk epoxy layer under the transparent ALD layer.

The viscosity of the liquid compound used in impregnation must be controlled precisely. If the viscosity is too high, it becomes necessary to use high pressure gradients to overcome the hydraulic resistance. This will complicate the manufacturing process. Vacuum impregnation is a well-known industrial process, and would probably be needed to ensure that no air bubbles remain in the AM prints. The use of high temperatures, to lower the viscosity, is problematic in many cases (Buevich and Kalinnikov 1979). Ideally, the properties of the liquid and the AM print would allow impregnation by capillary action.

Epoxy impregnation might bring additional benefits. For example, it is possible that elimination of the porosity with epoxy impregnation could improve the mechanical properties of an AM print, effectively creating a part made of *composite material*.

Results of Step 3 – ALD Al_2O_3 Coating

The applied top–coat layer was ALD Al_2O_3. There were no problems encountered during this coating process. The resulting Al_2O_3 layer was estimated to be approximately 95 nm thick, based on the actual ALD process parameters. After the coating, numerous surface microcracks were found when the test articles were examined with an optical microscope (Fig. 5). This was the case for the PC, PEEK and ND-PLA parts. The ABS parts appeared to have much less cracks, but because these parts were black, we suspect that the colour of the parts affected the visual inspection. These cracks in the ALD coating were evident in both the epoxy impregnated and non-impregnated parts.

As the main plastic material was fully covered under the epoxy film, it was the cured epoxy compound that controlled the ALD-related chemical reactions for the initial ALD layers, except for the three non-impregnated PC parts. Since the aim was to find an efficient manufacturing process, as few processing steps as possible were planned. For this reason, no surface pretreatment of the test articles was conducted before ALD. Depending on the material and the surface characteristics, a surface pretreatment may improve the quality of an ALD coating.

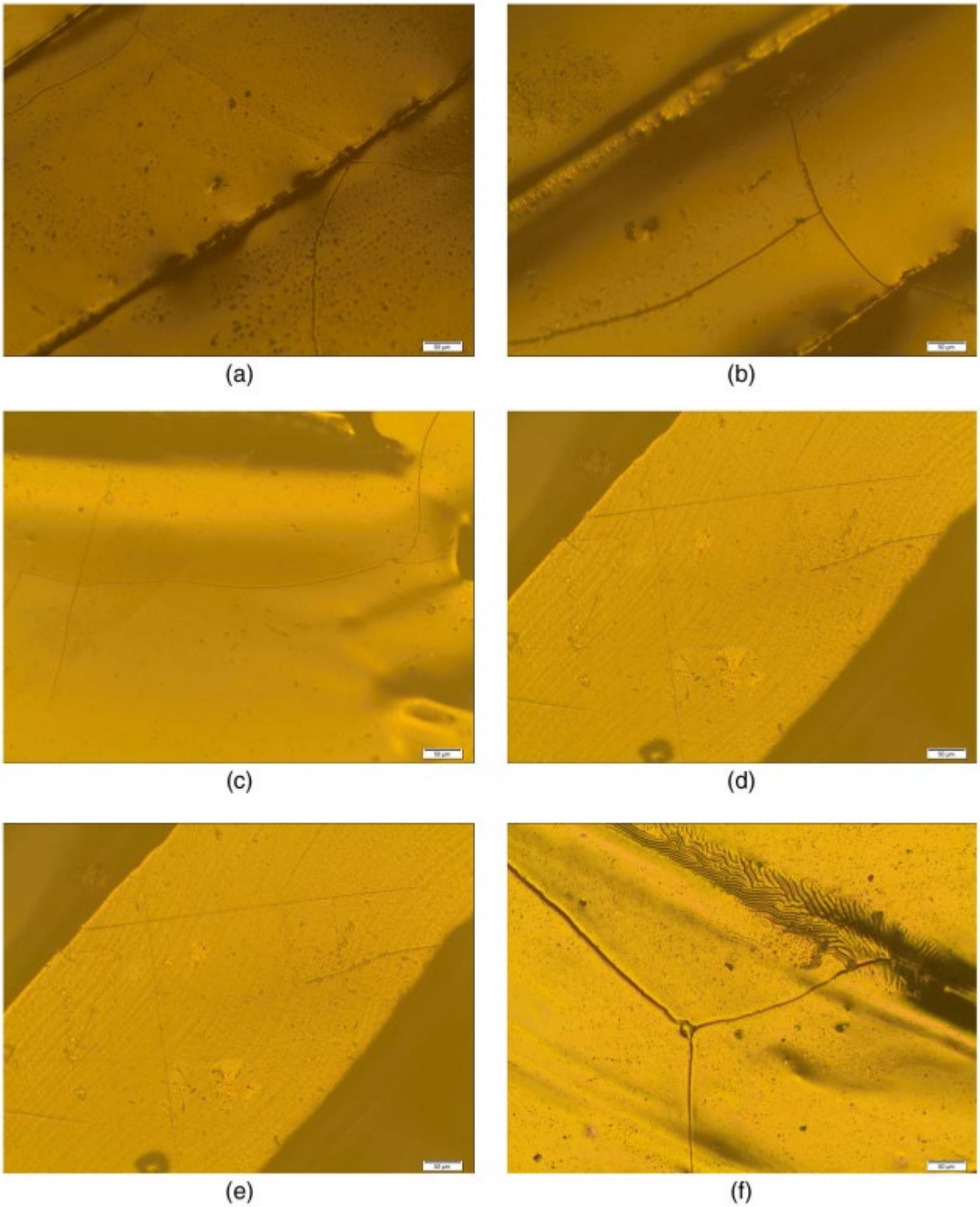

Figure 5. Images from visual inspection of the ALD coating with an optical microscope: (a) Test article A4 (PEEK); (b) A4 (PEEK); (c) A2 (PC) with epoxy impregnation; (d) A11 (PC) without impregnation (ALD coating on polymer substrate); (e) A6 (ND-PLA); and (f) B5 (ABS). Large scale tracks (approximately 400 μm) are features from material extrusion process. Thin lines (estimated 1–3 μm from the images) are cracks in the ALD Al2O3 thin-film coating, found in all coated test articles.

423 In addition to providing adhesion, the Al_2O_3 acts as a *barrier coating*. However, this requires

a sufficient layer thickness. The selection of a proper coating thickness for the ALD layers is important. With ALD Al_2O_3, a coating thickness of 100 nm is common. At least one study (Jen et al. 2011) has shown a smaller cracking tendency for thinner Al_2O_3 coatings.

The adhesion between the ALD coatings and substrates was not measured in this study. However, this type of adhesion has been previously evaluated for thermoplastics and epoxies (Chen et al. 2019). In order to test coating adhesion, a similar scratch test as explained by Bull could be used (Bull 1997).

Results of Step 4 – Thermal-Vacuum Outgassing Test

The results of our thermal–vacuum tests show a significant reduction in the outgassing of the ALD coated test articles. Compared to the uncoated parts, the ALD Al_2O_3 coating decreased the outgassing of PEEK by 46%; ABS, by 49%; PC, by 58%; and ND-PLA, by 65%.

As the PC part (A11) was lacking epoxy impregnation, the comparison of this substrate and the other three substrates is somewhat complicated (Table 3). The outgassing results of the impregnated PEEK, ABS and ND-PLA parts can be directly compared against each other, as they all had the epoxy impregnation and ALD coating. On the other hand, the outgassing results of the non-impregnated PC part (A11) clearly show that the presence of the ALD coating was the main reason for the reduced outgassing. Regarding the reference parts, all four were non-impregnated and without any ALD coating, printed from PEEK, ABS, PC and ND-PLA using the same AM process as used for the coated parts.

It is well known that all polymeric substances exhibit some level of outgassing, as absorbed gases, moisture and extraneous solvents egress. However, it is more important to detect and study the evaporation of substances related to the basic polymer structure itself (Muraca and Whittick 1967). For this reason, we chose to measure the outgassing using RGA. Fig. 6 and 7 report the measured outgassing of the TVC Test 1 and 2, respectively.

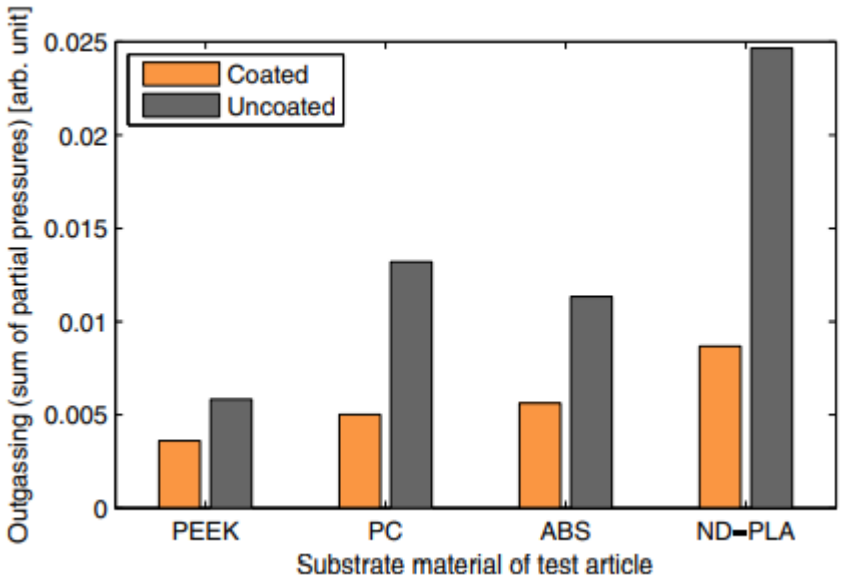

Figure 6. Outgassing of the test articles, measured by using the *coarse* resolution mode of the RGA during initial exposure to a vacuum (thermal-vacuum chamber Test 1). The constituents of N, N2, H2O, OH, and O2 were removed from the RGA data before analysis, because these are most likely traces of trapped ambient air and residuals of nitrogen gas used during chamber purging.

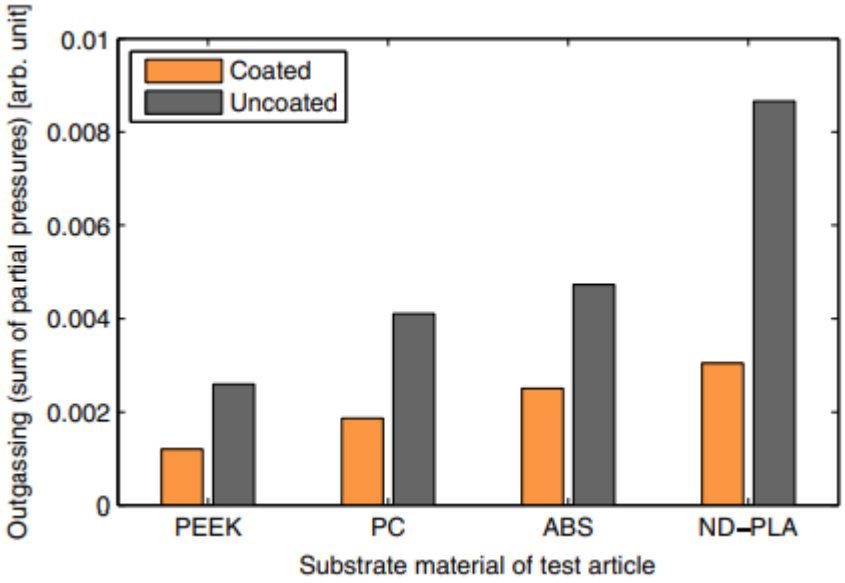

Figure 7. Outgassing of the test articles, measured by using the *fine* resolution mode of the RGA. The figure shows the results for the thermal-vacuum chamber Test 2. The constituents of N, N2, H2O, OH, and O2 were removed from the RGA data before analysis, because these are most likely traces of trapped ambient air and residuals of nitrogen gas used during chamber purging.

Qualitative analysis of the obtained RGA spectras should include: 1) fragmentation patterns; 2) multiply charged ions, and; 3) isotope ratios. For the uncoated ABS test article, the measured RGA spectra (Fig. 8) shows a distinct peak for ions with an atomic mass unit (AMU) of 40. This peak could be associated with 1,3-butadiene which is one constituent of ABS. However, this peak is

more likely associated with argon gas, especially when taking into account the lower peak at AMU 20 and the fact that the peak is also visible in the spectras of PEEK, PC and ND-PLA parts. No other peaks clearly associated with a polymer structure were detected. It is likely that the parts must be heated to higher temperatures before the outgassing of these polymer structures produce distinct peak patterns. Although our results clearly indicate a reduced outgassing rate for each of the coated test articles, a more comprehensive test campaign would be required to analyse the composition of the outgassed particles. This campaign would necessarily include elevated temperatures, at least 125 ˚C and possibly up to 250 ˚C for PEEK, in order to gain better knowledge of the behaviour of this type of components in various locations in a spacecraft. In this study and in future studies, the logarithmic RGA spectra (Fig. 8) is useful for the peak detection.

ALD coatings thicker than 10 nm can be used as a gas diffusion barrier (Jen et al. 2011). The type of ALD Al_2O_3 coating used in this study has been shown to be amorphous and having excellent gas barrier properties (Heidary and Randall 2015). This can effectively reduce the outgassing of many polymers in space. The coating will also protect the polymer from highly reactive atomic oxygen particles. Our findings support this.

In order to qualify this type of parts for the NASA or European Space Agency (ESA) missions, further outgassing testing is required. In the United States, the ASTM test methods E595 and E1559 are used to qualify materials for use in spacecraft, when it comes to outgassing (ASTM 2020). In Europe, the ECSS-Q-ST-70C standard lays out the criteria for space-grade materials, mechanical parts and processes. Related to outgassing, this document states that the ECSS-Q-ST-70-02C and ECSS-Q-TM-70-52A standards are relevant (ECSS 2020).

CONCLUSIONS

Research has shown many benefits of using AM for space applications. Recently, Rui Hu et al. studied an AM-enabled concept for the design of a space telescope primary mirror (Hu et al. 2016). In light of the topics covered above, we evaluated the manufacturing of thermoplastic parts for spacecraft, using a combined AM-ALD technique.

Most importantly, we showed a path towards creation of space-grade components using a

combination of AM and ALD. This type of manufacturing method enables the use of *topology optimization* already in the early concept creation phase. It is ideally suited for spacecraft applications, where the volume and mass of parts is often critical. In-space manufacturing using these methods could be applied to various use cases. Parts printed from PEEK, PC or ABS could be used for structural applications. Food packaging and general purpose items could be made from PLA, which is biocompatible and environmentally friendly.

In this study, we used two low viscosity epoxies for the impregnation of AM parts. Surface porosity was effectively removed. Interestingly, elimination of the porosity with epoxy impregnation could improve the mechanical properties of an AM print. This was not verified in our tests, but could be studied in future.

Although our results clearly demonstrate a reduction in outgassing, further testing is necessary to separate the effect of the impregnation and the effect of the ALD coating.

The main results of the presented analysis can be summarized as follows: 1) Significant reduction in outgassing was demonstrated. Low outgassing is one important criteria for the selection of spacecraft materials, and; 2) The inherent porosity of AM-MEX printed thermoplastic parts was effectively removed, at least near the surface, using epoxy impregnation.

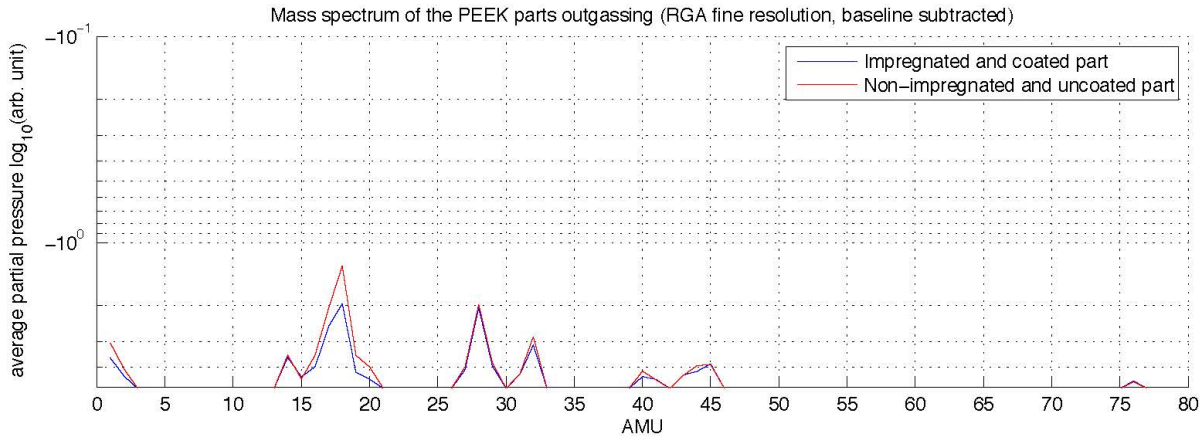
Mass spectrum of the PEEK parts outgassing (RGA fine resolution, baseline subtracted)
Impregnated and coated part
Non–impregnated and uncoated part
average partial pressure log10(arb. unit)
AMU

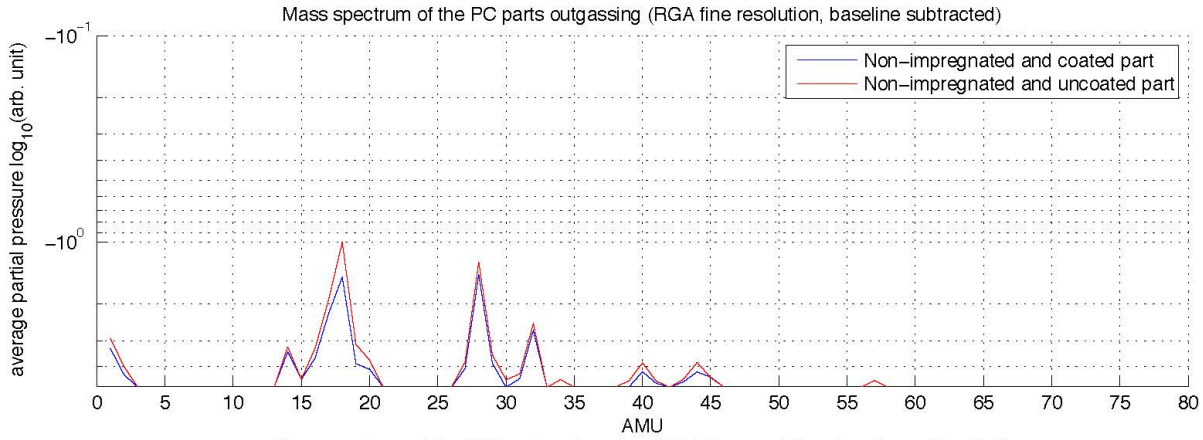
Mass spectrum of the PC parts outgassing (RGA fine resolution, baseline subtracted)
Non–impregnated and coated part
Non–impregnated and uncoated part
average partial pressure log10(arb. unit)
AMU

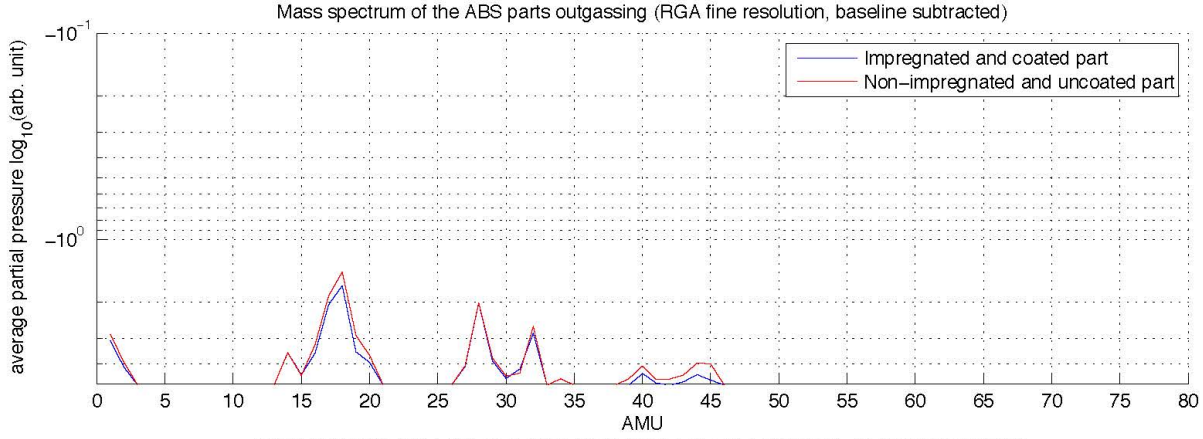
Mass spectrum of the ABS parts outgassing (RGA fine resolution, baseline subtracted)
Impregnated and coated part
Non–impregnated and uncoated part
average partial pressure log10(arb. unit)
AMU

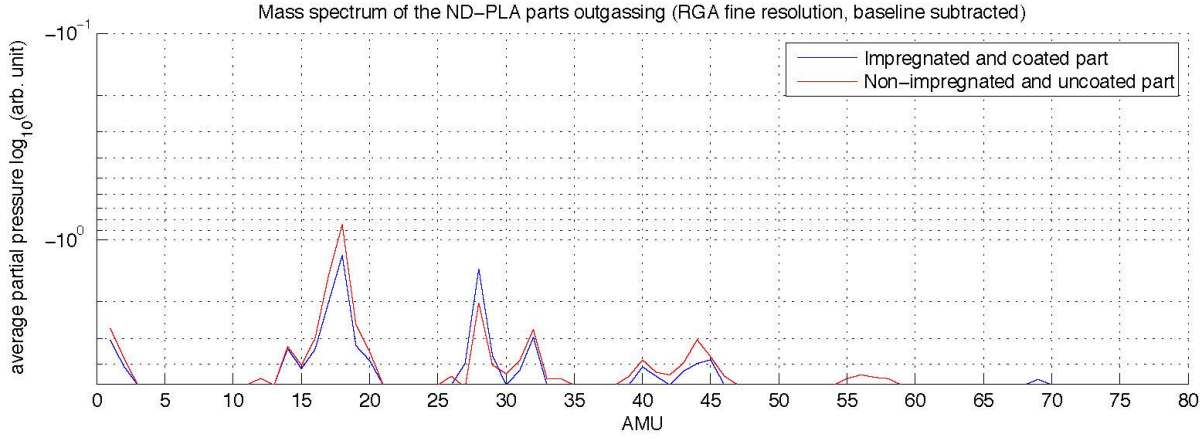
Mass spectrum of the ND–PLA parts outgassing (RGA fine resolution, baseline subtracted)
Impregnated and coated part
Non–impregnated and uncoated part
average partial pressure log10(arb. unit)
AMU

Figure 8. Mass spectrum plots of the RGA data up to AMU 80. Higher masses did not produce noticeable peaks. Chamber baseline measurement has been subtracted in these plots, to show the outgassing of the test articles solely.

DATA AVAILABILITY STATEMENT

Some or all data, models, or code generated or used during the study are available from the corresponding author upon request. This includes RGA measurements, laboratory notes and pictures.

ACKNOWLEDGEMENTS

We thank the European Space Agency (ESA) who has supported parts of this research as part of the HighPEEK project (ESA Contract N° 4000127834/19/UK/AB). In particular, Ugo Lafont and Paul Greenway (ESA) have our gratitude. We also deeply appreciate the help given by Daniel Leese (exchange student at Aalto University), Kirsi Kukko, Ashish Mohite and Olli Knuuttila (Aalto University), Lorenz Schmuckli and Pekka Rummukainen (Aalto University, retired) and Katja Väyrynen and Marko Vehkamäki (University of Helsinki).

REFERENCES

Abdulagatov, A., Yan, Y., Cooper, J., Zhang, Y., Gibbs, Z., Cavanagh, A., Yang, R., Lee, Y., and George, S. (2011). "Al2O3 and TiO2 atomic layer deposition on copper for water corrosion resistance.." *ACS applied materials & interfaces*, 3(12), 4593–4601.

ASTM (2020). "American Society for Testing and Materials., <https://www.astm.org>.

Broas, M. (2018). "Quality, microstructural refinement and stability of atomic-layer-deposited aluminum nitride and aluminum oxide films." Ph.D. thesis, Aalto University, Finland.

Buevich, Y. and Kalinnikov, V. (1979). "Impregnation of a heated filler with a viscous liquid." *Journal of Engineering Physics and Thermophysics*, 36(6).

Bull, S. (1997). "Failure mode maps in the thin film scratch adhesion test." *Tribology international*, 30(7), 491–498.

Chen, Y., Ginga, N., LePage, W., Kazyak, E., Gayle, A., Wang, J., Rodríguez, R., Thouless, M., and Dasgupta, N. (2019). "Enhanced interfacial toughness of thermoplastic–epoxy interfaces using ALD surface treatments.." *ACS Applied Materials & Interfaces*, 11(46), 43573–43580.

520 Cooper, R., Upadhyaya, H., Minton, T., Berman, M., Du, X., and George, S. (2008). "Protection of
521 polymer from atomic-oxygen erosion using Al2O3 atomic layer deposition coatings." *Thin Solid*
522 *Films*, 516(12), 4036–4039.
523 Cruise, A., Bowles, J., Patrick, T., and Goodall, C. (2006). *Principles of space instrument design*.
524 Cambridge University Press.
525 ECSS (2020). "European Coordination for Space Standardization., <https://www.ecss.nl>.
526 Fortescue, J., Swinerd, G., and Stark, J. (2011). *Spacecraft systems engineering*. John Wiley &
527 Sons, West Sussex.
528 Gilmore, D. (2003). *Spacecraft thermal control handbook*. Aerospace Press.
529 Grau, S. (2019). *Contributions to the Advance of the Integration Density of CubeSats*, Vol. 3.
530 Universitätsverlag der TU Berlin.
531 Groner, M., Fabreguette, F., Elam, J., and George, S. (2004). "Low-temperature Al2O3 atomic
532 layer deposition." *Chemistry of Materials*, 16(4), 639–645.
533 Grossman, E. and Gouzman, I. (2003). "Space environment effects on polymers in low earth
534 orbit." *Nuclear Instruments and Methods in Physics Research Section B: Beam Interactions with*
535 *Materials and Atoms*, 208, 48–57.
536 Heidary, D. and Randall, C. (2015). "Evaluating the merit of ALD coating as a barrier against
537 hydrogen degradation in capacitor components.." *RSC Advances*, 5(63), 50869–50877.
538 Hu, R., Chen, W., Li, Q., Liu, S., Zhou, P., Dong, Z., and Kang, R. (2016). "Design optimization
539 method for additive manufacturing of the primary mirror of a large-aperture space telescope."
540 *Journal of Aerospace Engineering*, 30(3).
541 Jen, S., Bertrand, J., and George, S. (2011). "Critical tensile and compressive strains for cracking
542 of Al2O3 films grown by atomic layer deposition." *Journal of Applied Physics*, 109(8).
543 Johnson, P., Copeland, P., Ayodele, A., Tarekegn, E., Bromley, S., Harrell, W., Sosolik, C., and
544 Marler, J. (2020). "In-vacuum performance of a 3D-printed ion deflector." *Vacuum*, 172, 109061.
545 Johnson, R., Hultqvist, A., and Bent, S. (2014). "A brief review of atomic layer deposition: from
546 fundamentals to applications.." *Materials today*, 17(5), 236–246.
547 Kestilä, A., Nordling, K., Miikkulainen, V., Kaipio, M., Tikka, T., Salmi, M., Auer, A., Leskelä, M.,

548 and Ritala, M. (2018). “Towards space-grade 3D-printed, ALD-coated small satellite propulsion
549 components for fluidics.” *Additive Manufacturing*, 22, 31–37.
550 Kirn, T. (2013). “The AMS-02 TRD on the international space station..” *Nuclear Instruments and*
551 *Methods in Physics Research Section A: Accelerators, Spectrometers, Detectors and Associated*
552 *Equipment*, 706, 43–47.
553 Krzysztof, M., Kubera, H., Głuszewski, W., and Zimek, Z. (2011). “Effect of ionizing radiation on
554 the properties of PLA packaging materials.” *Nukleonika*, 56, 65–69.
555 Kutilainen, T., Pudas, M., Ashworth, M., Lehto, T., Wu, L., Wilcox, G., Wang, J., Collander, P., and
556 Hokka, J. (2019). “Atomic layer deposition (ALD) to mitigate tin whisker growth and corrosion
557 issues on printed circuit board assemblies.” *Journal of Electronic Materials*, 48(11), 7573–7584.
558 Kutz, M. (2002). *Handbook of materials selection*. John Wiley & Sons.
559 Lanouette, A., Potvin, M., Martin, F., Houle, D., and Therriault, D. (2015). “Residual mechanical
560 properties of a carbon fibers/PEEK space robotic arm after simulated orbital debris impact.”
561 *International Journal of Impact Engineering*, 84, 78–87.
562 Mark, J. (2009). *Polymer data handbook*. Oxford University Press.
563 McGuigan, A., Briggs, G., Burlakov, V., Yanaka, M., and Tsukahara, Y. (2003). “An elastic-plastic
564 shear lag model for fracture of layered coatings.” *Thin Solid Films*, 424(2), 219–223.
565 Minton, T., Wu, B., Zhang, J., Lindholm, N., Abdulagatov, A., O’Patchen, J., George, S., and
566 Groner, M. (2010). “Protecting polymers in space with atomic layer deposition coatings.” *ACS*
567 *applied materials & interfaces*, 2(9), 2515–2020.
568 Muraca, R. and Whittick, J. (1967). “Polymers for spacecraft applications..” *Report No. N67-40270*,
569 Stanford Research Institute.
570 Murari, A., Vinante, C., and Monari, M. (2002). “Comparison of PEEK and VESPEL SP1 charac-
571 teristics as vacuum seals for fusion applications..” *Vacuum*, 65(2), 137–145.
572 Nogales, C., Grim, B., Kamstra, M., Campbell, B., Ewing, A., Hance, R., Griffin, J., and Parke,
573 S. (2018). “MakerSat-0: 3D-printed polymer degradation first data from orbit.” *32th Annual*
574 *AIAA/USU Conference on Small Satellites*.
575 Prater, T., Edmunson, J., Ledbetter, F., Fiske, M., Hill, C., Meyyappan, M., Roberts, C., Huebner,

L., Hall, P., and Werkheiser, N. (2019). "NASA's in-space manufacturing project: Update on manufacturing technologies and materials to enable more sustainable and safer exploration." *70th International Astronautical Congress (IAC), Washington, D.C., 21-25 October 2019*.

Rückerl, A., Zeisel, R., Mandl, M., Costina, I., Schroeder, T., and Zoellner, M. (2017). "Characterization and prevention of humidity related degradation of atomic layer deposited Al2O3." *Journal of Applied Physics*, 121(2).

Shulman, H. and Ginell, W. (1970). "Nuclear and space radiation effects on materials." *Report No. SP-8053*, NASA.

Stein, B. (1992). "An interim overview of LDEF materials findings." *Report No. 107664*, NASA.

Stein, B. (1993). "LDEF materials overview." *Report No. 93-28255*, NASA.

Tynell, T. and Karppinen, M. (2014). "Atomic layer deposition of ZnO: a review." *Semiconductor Science and Technology*, 29(4), 043001.

Varadan, V., Xiaoning, J., and Varadan., V. (2001). *Microstereolithography and other fabrication techniques for 3D MEMS*. John Wiley and Sons, New Jersey.

VTT (2018). "VTT and Carbodeon speed up 3D printing with nanodiamonds (accessed: 12.07.2020), <https://www.vttresearch.com/en/news-and-ideas/vtt-and-carbodeon-speed-3d-printing-nanodiamonds>.

Zanjanijam, A., Major, I., Lyons, J., Lafont, U., and Devine, D. (2020). "Fused filament fabrication of PEEK: A review of process-structure-property relationships." *Polymers*, 12(8), 1665.